nature materials

LETTERS

PUBLISHED ONLINE: 3 AUGUST 2014 | DOI: 10.1038/NMAT4046

A time-dependent order parameter for ultrafast photoinduced phase transitions

P. Beaud[1,2*], A. Caviezel[1], S. O. Mariager[1], L. Rettig[1], G. Ingold[1,2], C. Dornes[3], S-W. Huang[1], J. A. Johnson[1], M. Radovic[1,2], T. Huber[3], T. Kubacka[3], A. Ferrer[1,3], H. T. Lemke[4], M. Chollet[4], D. Zhu[4], J. M. Glownia[4], M. Sikorski[4], A. Robert[4], H. Wadati[5,6], M. Nakamura[7], M. Kawasaki[5,7], Y. Tokura[5,7], S. L. Johnson[3] and U. Staub[1]

Strongly correlated electron systems often exhibit very strong interactions between structural and electronic degrees of freedom that lead to complex and interesting phase diagrams[1,2]. For technological applications of these materials it is important to learn how to drive transitions from one phase to another. A key question here is the ultimate speed of such phase transitions, and to understand how a phase transition evolves in the time domain[3–13]. Here we apply time-resolved X-ray diffraction to directly measure the changes in long-range order during ultrafast melting of the charge and orbitally ordered phase in a perovskite manganite. We find that although the actual change in crystal symmetry associated with this transition occurs over different timescales characteristic of the many electronic and vibrational coordinates of the system, the dynamics of the phase transformation can be well described using a single time-dependent 'order parameter' that depends exclusively on the electronic excitation.

The concept of an order parameter was introduced by Landau and Lifshitz to characterize phase transitions in the adiabatic limit[14]. Typically, a phase transition is characterized by a change of the order parameter from zero to a non-zero finite value as a function of a slowly changing thermodynamic state variable. The order parameter is a measure of symmetry breaking in the equilibrium state. The Landau free energy $F(\eta)$ is a phenomenological expression of the free energy of a system at a fixed value of the order parameter η. Near the phase transition, η is small, allowing $F(\eta)$ to be approximated by the first terms of a Taylor expansion in η. The equilibrium value of the order parameter η is given by the minimum of $F(\eta)$. Assuming simple relations between thermodynamic state variables and the Taylor coefficients provides a highly useful description of many types of commonly encountered phase transitions.

In real physical situations we rarely have the possibility of making truly adiabatic changes to induce phase transitions. An extreme example is the so-called 'ultrafast' phase transition, where a persistent symmetry change is induced by a sudden impulsive interaction from a laser pulse lasting only a few femtoseconds[3–13]. In this case, different coordinates of the phase transformation, that in equilibrium are tightly linked to the conventionally defined order parameter, can undergo quite different dynamics. Whether a unified explanation of such dynamics exists remains an open question.

To address this issue, we investigated the dynamics of the ultrafast phase transition in an epitaxially grown film of $Pr_{0.5}Ca_{0.5}MnO_3$ (PCMO), a perovskite-type manganite, a class of systems which exhibits properties such as colossal magnetoresistance and insulator-to-metal transitions that are intrinsically related to symmetry changes of the atomic lattice and to intriguing ordering patterns of the spins, orbitals and charges[2,15]. Although much progress has been made in understanding the various schemes of magnetic, charge and orbital ordering and their relationship to the lattice, comparatively little is known about the interactions among these different degrees of freedom. Investigations of photoexcited manganites using optical probes suggest that the electronic properties change on a timescale faster than the period of the Jahn–Teller mode of 70 fs (refs 4,16). Complementary to optical probes, diffraction techniques yield a direct and quantitative measurement of the long-range order[6,8,10,11,13]. Employing femtosecond X-ray diffraction (XRD) it has been shown that the change of lattice symmetry occurs on a slower but still subpicosecond timescale[6,17].

Here we employ femtosecond XRD, which when tuned to a resonance offers, in addition to the lattice dynamics, information on the long-range charge and orbital order (COO; ref. 18). Taking advantage of the high X-ray flux of a free-electron laser (FEL; ref. 19) we are able to measure different classes of superlattice reflections, each sensitive to a specific component of the phase transition. We classify these into three categories (in *Pbnm* notation with k odd): one type of reflection ($0\ k/2\ 0$) is sensitive directly to the orbital order and Jahn–Teller distortion, a second type ($0\ k\ 0$) is more sensitive to the charge order, and a general type ($h\ k/2\ l$) measures predominantly the overall structural distortion[18]. Figure 1a shows a schematic of the optical-pump X-ray-probe experiment. Experimental details are given in the Methods. 1.55 eV photons mainly excite the Mn^{3+} intra-site transition[20], which drives the relaxation of the Jahn–Teller distortion (Fig. 1b,c).

Time-resolved XRD data for various reflections are shown in Fig. 2a–c. The observed dynamics for lower pump fluences are dominated by a strong 2.45 THz oscillation, which is the slowest of a series of coherent optical phonon modes observed when these materials are excited with very short optical pulses[21]. Faster components can be inferred from the changes observed at early times, although the time resolution is insufficient to resolve them. At late times, the disappearance of the superlattice reflections

[1]Swiss Light Source, Paul Scherrer Institut, 5232 Villigen PSI, Switzerland, [2]SwissFEL, Paul Scherrer Institut, 5232 Villigen PSI, Switzerland, [3]Institute for Quantum Electronics, ETH Zürich, 8093 Zürich, Switzerland, [4]LCLS, SLAC National Accelerator Laboratory, Menlo Park, California 94025, USA, [5]Department of Applied Physics and Quantum-Phase Electronics Center, University of Tokyo, Hongo, Tokyo 113-8656, Japan, [6]Institute for Solid State Physics, University of Tokyo, Kashiwanoha 5-1-5, Chiba 277-8581, Japan, [7]RIKEN Center for Emergent Matter Science (CEMS), Wako 351-0198, Japan. *e-mail: paul.beaud@psi.ch

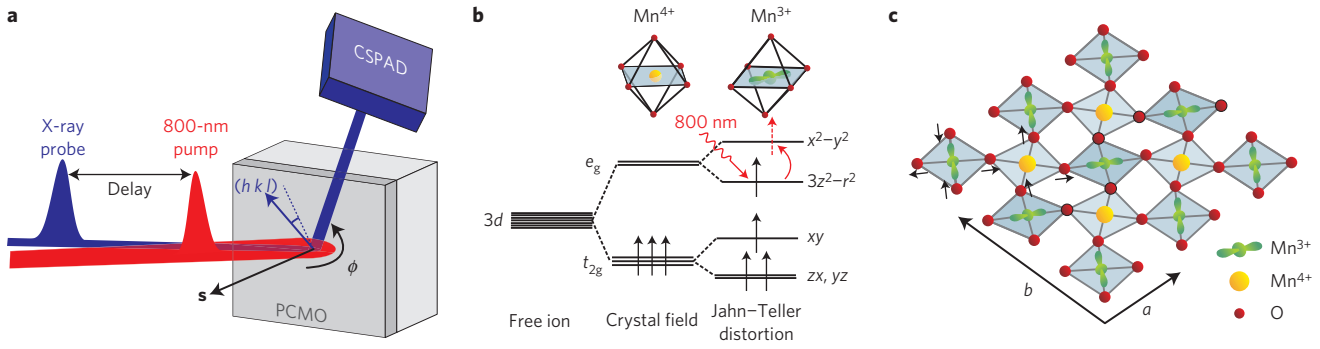

Figure 1 | Ultrafast melting of charge and orbital order. a, Schematic set-up of the optical-pump/X-ray-probe experiment. In the asymmetric diffraction configuration the sample is rotated by an angle ϕ around its surface normal **s** to fulfil the Bragg condition for a given reflection (h k l). CSPAD, Cornell-SLAC hybrid Pixel Array Detector[29]; PCMO, $Pr_{0.5}Ca_{0.5}MnO_3$. **b**, In the cubic crystal field the degenerate Mn 3*d* states are split into the e_g and t_g bands. In the ground state, distortions of the oxygen octahedra at the Mn^{3+} sites further split the bands (Jahn–Teller effect). **c**, On cooling to the ground state charge and orbital order is observed alongside with a Jahn–Teller distortion of the $Mn^{3+}O_6$ octahedra, leading to a doubling of the unit cell along the *b* axis and a symmetry change from orthorhombic *Pbnm* to monoclinic $P2_1/m$ (ref. 30). The staggered configuration of the Mn^{3+} sites along *b* is accompanied by the ordering of the elongated Mn^{3+} 3*d* $3z^2$–r^2 orbitals[15]. The black arrows show the motion of the Jahn–Teller mode for one Mn^{3+}/Mn^{4+} pair.

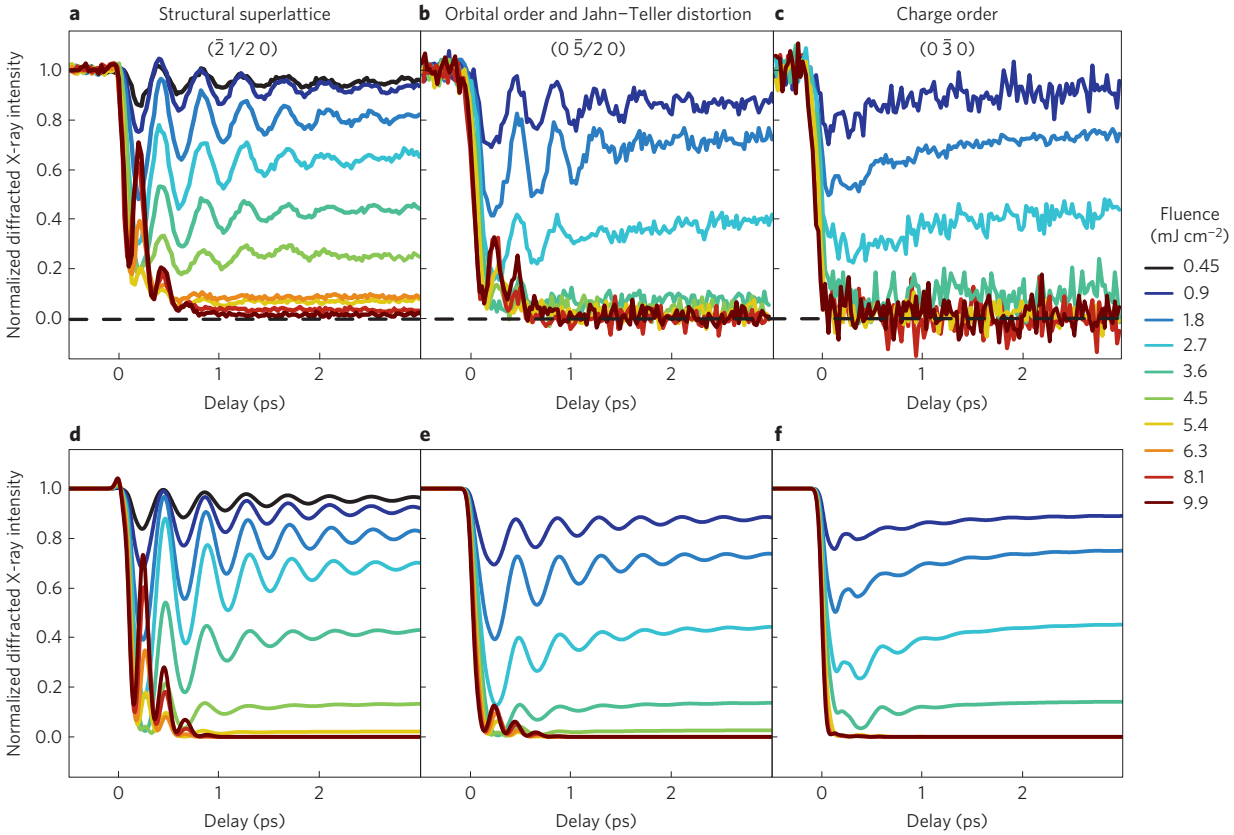

Figure 2 | Measured (top) and simulated (bottom) evolution of the normalized diffracted X-ray intensity for three superlattice reflections. a,**d**, The ($\bar{2}$ 1/2 0) reflection off resonance at 6.53 keV, which is sensitive only to the structural atomic motion. **b**,**e**, The (0 $\bar{5}$/2 0) reflection is only slightly enhanced by ~15% at resonance (6.553 keV) and therefore mainly sensitive to the Jahn–Teller distortion. **c**,**f**, The (0 $\bar{3}$ 0) reflection at 6.555 keV is strongly resonantly enhanced by a factor of ~4 and mainly sensitive to the electronic order. The fluence required to suppress the Bragg peaks varies for the different reflections simply because of the birefringence of the material (Supplementary Information). The model used to generate the simulated curves **d**–**f** is discussed in the manuscript.

at high pump fluences is unambiguous evidence that the lattice symmetry has changed. Even before this, the observed doubling of the oscillation frequency in the diffracted signal is evidence of another kind of symmetry change in the potential energy surface: the atoms coherently oscillate with a frequency of ~2.45 THz over the equilibrium positions of a higher-symmetry lattice. These oscillations persist for a short time before the coherent motions relax and the phase transition is completed.

To gain a better understanding of the fluence dependent dynamics we first discuss the behaviour of the $(0\bar{3}0)$ reflection (Fig. 2c), which at resonance is predominantly a measure of the charge order. If we assume that the purely electronic degrees of

freedom thermalize within our time resolution, we can define an effective 'time-dependent order parameter' η_t that gives a measure of the symmetry breaking of the electronic system at a particular time t. We can therefore identify η_t with the structure factor $F^{0\bar{3}0}$ of the $(0\bar{3}0)$ reflection.

Within the accuracy of the experiment we find that the diffracted X-ray intensity $I^{hkl} = |F^{hkl}|^2$ averaged in the 250–500 fs time interval drops linearly with fluence until it vanishes at ~4 mJ cm^{-2} (Fig. 3, red curve). At 250–500 fs after excitation we then have $\eta_t = \sqrt{1-n_0/n_c}$ for an absorbed energy density n_0 less than a critical energy density n_c. Here we have normalized η_t to unity at times before excitation. For $n_0 > n_c$ the phase transition takes place and $\eta_t = 0$. The optical absorption length at 800 nm is on the order of the film thickness. To quantitatively describe the fluence-dependent data we account for the inhomogeneity of the excitation $n_0(z)$ by dividing the film into N slices along the depth z (Supplementary Information) and compute the structure factor $F^{0\bar{3}0} = 1/N \sum \eta_t(z_i)$.

For $n_0 < n_c$ the fast change in electronic order induced by the excitation pulse partially recovers within a few picoseconds (Fig. 2c), reaching a quasi-equilibrium state empirically well described by $\eta_t = (1-n_0/n_c)^{\gamma}$ (Fig. 3, blue curve). The observed recovery of charge order may be attributed to energy transfer from the initially excited electron system to the lattice. Generalizing the relation between η_t and n found above we define a time-dependent order parameter:

$$\eta_t(t) = \sqrt{1-n(t)/n_c} \quad (1)$$

For $n_0 < n_c$ we can then empirically describe the evolving electronic energy density by

$$n(t) = (n_0 - \alpha n_c)\, e^{-t/\tau} + \alpha n_c \quad (2)$$

with $\alpha = 1-(1-n_0/n_c)^{2\gamma}$. Here τ is an effective relaxation time and γ is analogous to a critical exponent of the initial excitation. A fit to the $(0\bar{3}0)$ intensity based on equations (1) and (2) is superimposed on the data in the inset of Fig. 3, yielding $\gamma = 0.21(1)$, $\tau = 0.81(4)$ ps and $n_c = 477(7)$ J cm^{-3} (≈1.33 eV per unit cell).

The full phase transition requires not only a symmetry change in the charge distribution, but also a motion of the atoms to a higher-symmetry site position that is coherently driven by electronic excitation via a fast change of the atomic potential[3,7,12,13]. Here the rapid laser-induced melting of charge and orbital order releases the forces that stabilize the Jahn–Teller lattice distortions at the Mn^{3+} sites[4,6,16,17]. This sudden release of force triggers a chain reaction that couples to other vibrational modes, leading to a rearrangement of the atoms in the unit cell.

The timescales of this atomic motion are determined by the eigenmodes of the lattice[3,4,8,21]. In Fig. 2a, we clearly see that the dynamics involve oscillatory motions around a quasi-equilibrium position. In view of the complicated atomic structure of PCMO and our limited knowledge of the eigenmodes, an exact treatment of the structural dynamics is not feasible. In our model we approximate the atomic motions relevant to the phase transition to four groups of effective modes and we make the following ansatz for the time-dependent atomic potential:

$$V(t) = -\frac{a}{2}\left(1-\frac{n(t)}{n_c}\right) y_1^2 + \frac{b}{4} y_1^4 + \frac{c_{21}}{2}(y_2-y_1)^2 + \frac{c_{32}}{2}(y_3-y_2)^2 + \frac{c_{43}}{2}(y_4-y_3)^2 \quad (3)$$

Here y_i are atomic motion coordinates relevant to the structural symmetry change defined in Fig. 4. The coefficients a, b and c_{ij} are energies that depend mainly on the respective phonon frequencies and atomic masses. The amplitudes are normalized such that $y_i = 1$ before arrival of the pump pulse. The double-well potential given by the first two terms in equation (3) accounts for the electronic excitation[7] and for modes that are directly related to the Jahn–Teller distortion: the Jahn–Teller and the breathing mode. The last three terms account for atomic motion coherently excited during the subsequent relaxation process. Identifying y_1 with the primary order parameter for the structural distortion, equation (3) corresponds to the result of Landau theory for a second-order phase transition with T/T_c substituted by n/n_c. This functional form of the potential ensures that at any time t the minimum of the potential is given for $y_i = \eta_t$ $(i = 1 \ldots 4)$. The fast change in $n(t)$ induced by the optical pulse launches the coherent oscillatory atomic motions and $y_i(t) \to \eta_t(t)$ for $t \gg \tau$.

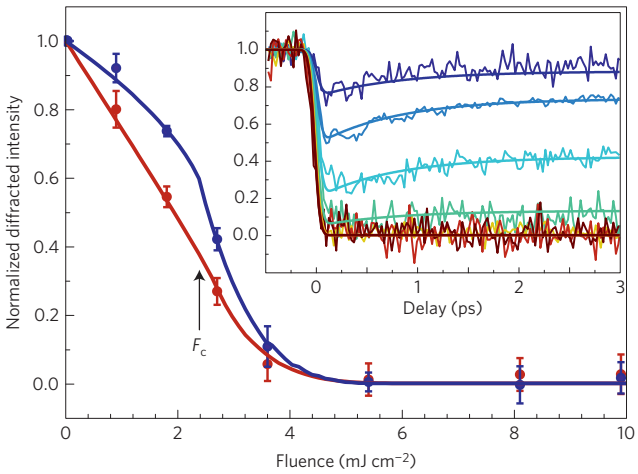

Figure 3 | Fluence dependence of charge order dynamics. Here we exploit that the $(0\bar{3}0)$ reflection predominantly measures the charge order and neglect the small oscillations in the diffracted intensity visible at lower fluences. Red symbols: fluence dependence of the reflection averaged over an early 0.25–0.5 ps time window. The error bars represent standard deviation. The fit (red curve) using $F^{hkl} \propto \sqrt{1-n_0/n_c}$ yields $n_c = 521(19)$ J cm^{-3}. The arrow marks the fluence F_c corresponding to n_c, where the topmost layer of the film proceeds with the phase transition. Because of a strong depth gradient in the excitation profile, the fluence needed to completely suppress the diffraction peak for the entire film thickness exceeds F_c by a factor of approximately 2.3. Blue symbols: fluence dependence averaged for a late window of 2.5–3 ps, which is well described by $F^{hkl} \propto (1-n_0/n_c)^{\gamma}$ with $\gamma = 0.20(2)$. Inset: Fits to the time-dependent charge order reflection using equations (1) and (2) with $F^{hkl} = \eta_t$.

We use equations of motion based on equation (3) to model the structural dynamics and to simulate the diffracted intensities (Supplementary Information). The simulated structural responses of the three reflections in Fig. 2a–c are shown in Fig. 2d–f. Despite the drastic simplifications the main features of the observed rich structural dynamics are well reproduced. In particular, we have neglected the significant resonant enhancement from charge order to the $(0\bar{3}0)$ reflection. The good agreement between the measured and simulated response for this reflection is indicative of the intrinsic cooperative charge, orbital and atomic order in this material.

The structural transition observed here within the first few picoseconds does not correspond to the full phase transition from monoclinic $P2_1/m$ to the orthorhombic $Pbnm$ lattice observed at higher temperatures in equilibrium. Owing to their long-range character the required changes of the unit cell lattice constants and the monoclinic angle to reach the final $Pbnm$ lattice cannot occur on this timescale. It is limited by δ/c_s, where $c_s \approx 5$ nm ps^{-1} is the speed of sound and $\delta \approx 75$ nm (ref. 22) the size of individual domains. Using an average specific heat[23] $c_p/T \approx 0.475$ J K^{-2} mol^{-1},

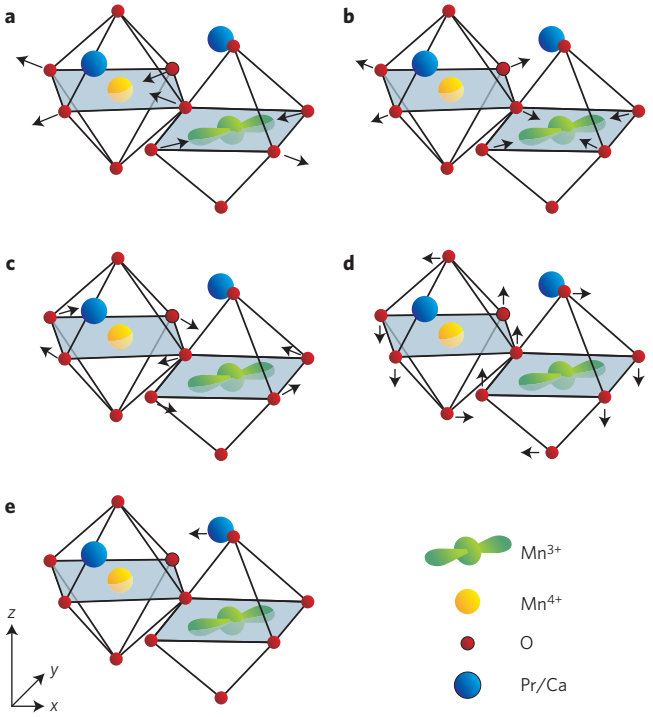

Figure 4 | Optical phonon modes related to the charge and orbital order phase. a,**b**, Melting of charge and orbital order directly excites the Jahn–Teller mode (**a**) and the breathing mode (**b**). **c**,**d**, Rotational modes. **e**, The slowest mode, with frequency ~2.5 THz, has been assigned solely to the motion of the rare earth cations[31]. Coherent excitation of the modes shown in **a**,**c**–**e** has been observed[21]. In our simplified model (equation (3)) y_1 combines the motion of the Jahn–Teller mode (**a**) and breathing mode (**b**) into one, y_2 corresponds to the motion of the Mn^{4+} atoms, their apex oxygens and a fraction of the motion of the rare earth cations, y_3 includes all remaining motions of the Mn^{3+} site oxygens (including those shown in **c**,**d**) and y_4 (corresponding to the mode in **e**) accounts for the remaining motion of the rare earth cations not accounted for by y_2.

we estimate that at an excitation corresponding to $n_c = 477\,\mathrm{J\,cm^{-3}}$ approximately 50% more energy is added to the system than needed to heat the sample to $T_{COO} \approx 220\,\mathrm{K}$. At excitation densities significantly below n_c the system is therefore trapped in a non-thermal ordered state which will vanish once the transition to the *Pbnm* lattice has completed[6,24].

So far we have ignored the spin lattice, which is an important although not indispensable ingredient of the physics of charge and orbitally ordered manganites as $T_N < T_{COO}$ (ref. 25). Although in our experiment the dynamics of the spin lattice cannot be measured, this dynamics should also relate to our time-dependent order parameter model. The melting of the magnetic order may occur very fast, as observed for the charge and orbital ordered layered $La_{0.5}Sr_{1.5}MnO_4$ system[10].

Here we have shown that resonant X-ray diffraction combined with the high flux and short pulse duration of a free-electron laser offers a unique opportunity to directly measure the non-equilibrium dynamics of the intertwined order parameters in half-doped PCMO, a prototypical example of a strongly correlated electron system. Despite the complex nature of this phase transition, which involves symmetry changes of valence charge, orbital order and atomic structure, a fairly simple description relying on a single time-dependent order parameter η_t is sufficient to capture the most essential aspects of the change in symmetry in the time domain down to ~80 fs. The lattice dynamics all occur in a potential surface defined by the magnitude of this single parameter. The resemblance of this description to Landau theory (replacing T/T_c by n/n_c) points towards a possible new universal description of complex phase transitions in the time domain. For example, very recently, van Veenendaal has presented a theory of the photoinduced metal–insulator transition in VO_2 in terms of a coherent motion of V–V dimers driven by electronic excitation beyond a certain critical level[26]. Although this work does not explicitly invoke a time-dependent order parameter η_t to describe the process, it seems likely that such a description could be made. In general, we would expect that the functional dependence of η_t could be used for a variety of photoinduced phase transitions in strongly correlated electron systems with coupled electronic and lattice degrees of freedom[3–13], but with parameters n_c, γ and τ that depend strongly on both the material and the underlying physics of the transition.

Methods

Sample preparation and characterization. The (011)-oriented $Pr_{0.5}Ca_{0.5}MnO_3$ thin film of approximately 40 nm thickness was grown on (011)-oriented $(LaAlO_3)_{0.3}$–$(SrAl_{0.5}Ta_{0.5}O_3)_{0.7}$ (LSAT) using a pulsed laser deposition technique with a laser pulse frequency of 2 Hz at 850 °C in an oxygen pressure of 1.5 mTorr (ref. 22). During the experiment the sample temperature was held at 100 K, well below $T_{COO} \approx 220\,\mathrm{K}$, using a cryogenic nitrogen blower. Static X-ray diffraction experiments to characterize the sample were performed at the X04SA beam line at the Swiss Light Source, Paul Scherrer Institut (Supplementary Information).

Time-resolved diffraction experiment. The experiment was performed at the X-ray Pump–Probe (XPP) instrument at the Linac Coherent Light Source (LCLS) at the SLAC National Accelerator Laboratory[19]. The experimental set-up is depicted schematically in Fig. 1a. A weakly focused (230 × 230 μm²) 55 fs optical pulse with a wavelength of 800 nm excited the sample with a repetition rate of 120 Hz at an incidence angle of 14° (*p*-polarization). An asymmetric diffraction configuration[27] was used to probe the laser-induced structural changes. The horizontally polarized 50 fs X-ray probe pulses were focused to a spot size of 50 × 34 μm² and entered the film at 8° grazing incidence. The X-ray energy was tuned in the vicinity of the Mn *K* edge using a silicon (111) monochromator. The inevitable jitter between pump and probe pulses was measured shot-by-shot using the spectral encoding correlation technique, which has an accuracy of ~15 fs (full-width at half-maximum; ref. 28). This information was then used to re-bin the data, significantly improving the time resolution (Supplementary Information).

Received 10 February 2014; accepted 1 July 2014; published online 3 August 2014

References

1. Dagotto, E. Correlated electrons in high temperature superconductors. *Rev. Mod. Phys.* **66,** 763–840 (1994).
2. Imada, M., Fujimori, A. & Tokura, Y. Metal–insulator transitions. *Rev. Mod. Phys.* **70,** 1039–1263 (1998).
3. Cavalleri, A. *et al.* Femtosecond structural dynamics in VO_2 during an ultrafast solid-solid phase transition. *Phys. Rev. Lett.* **87,** 237401 (2001).
4. Polli, D. *et al.* Coherent orbital waves in the photo-induced insulator-metal dynamics of a magnetoresistive manganite. *Nature Mater.* **6,** 643–647 (2007).
5. Schmitt, F. *et al.* Transient electronic structure and melting of a charge density wave in $TbTe_3$. *Science* **321,** 1649–1652 (2008).
6. Beaud, P. *et al.* An ultrafast structural phase transition driven by photo-induced melting of charge and orbital order. *Phys. Rev. Lett.* **103,** 155702 (2009).
7. Yusupov, R. *et al.* Coherent dynamics of macroscopic electronic order through a symmetry breaking transition. *Nature Phys.* **6,** 681–684 (2010).
8. Eichberger, M. *et al.* Snapshots of cooperative atomic motions in the optical suppression of charge density waves. *Nature* **468,** 799–802 (2010).
9. Rohwer, T. *et al.* Collapse of long-range charge order tracked by time-resolved photoemission at high momenta. *Nature* **471,** 490–493 (2011).
10. Först, M. *et al.* Driving magnetic order in a manganite by ultrafast lattice excitation. *Phys. Rev. B* **84,** 241104(R) (2011).
11. Johnson, S. L. *et al.* Femtosecond dynamics of the collinear-to-spiral antiferromagnetic phase transition in CuO. *Phys. Rev. Lett.* **108,** 037203 (2012).
12. Wall, S. *et al.* Ultrafast changes in lattice symmetry probed by coherent phonons. *Nature Commun.* **3,** 721 (2012).
13. De Jong, S. *et al.* Speed limit of the insulator–metal transition in magnetite. *Nature Mater.* **12,** 882–886 (2013).
14. Landau, L. D. & Lifschitz, E. M. *Statistische Physik* (Akademie-Verlag, 1987).

15. Tokura, Y. & Nagaosa, N. Orbital physics in transition-metal oxides. *Science* **288,** 462–468 (2000).
16. Singla, R. *et al.* Photoinduced melting of the orbital order in $La_{0.5}Sr_{1.5}MnO_4$ measured with 4-fs laser pulses. *Phys. Rev. B* **88,** 075107 (2013).
17. Caviezel, A. *et al.* Identifying coherent lattice modulations coupled to charge and orbital order in a manganite. *Phys. Rev. B* **87,** 205104 (2013).
18. Zimmermann, M. V. *et al.* Interplay between charge, orbital, and magnetic order in $Pr_{1-x}Ca_xMnO_3$. *Phys. Rev. Lett.* **83,** 4872–4875 (1999).
19. Emma, P. *et al.* First lasing and operation of an ångstrom-wavelength free-electron laser. *Nature Photon.* **4,** 641–647 (2010).
20. Jung, J. H. *et al.* Midgap states of $La_{1-x}Ca_xMnO_3$: Doping-dependent optical-conductivity studies. *Phys. Rev. B* **57,** R11043 (1998).
21. Matsuzaki, H. *et al.* Detecting charge and lattice dynamics in photoinduced charge-order melting in perovskite-type manganites using a 30-femtosecond time resolution. *Phys. Rev. B* **79,** 235131 (2009).
22. Okuyama, D. *et al.* Epitaxial-strain effect on charge/orbital order in $Pr_{0.5}Ca_{0.5}MnO_3$ films. *Appl. Phys. Lett.* **95,** 152502 (2009).
23. Smolyaninova, V. N. *et al.* Anomalous field-dependent specific heat in charge-ordered $Pr_{1-x}Ca_xMnO_3$ and $La_{0.5}Ca_{0.5}MnO_3$. *Phys. Rev. B* **62,** 6093–6096 (2000).
24. Ichikawa, H. *et al.* Transient photoinduced 'hidden' phase in a manganite. *Nature Mater.* **10,** 101–105 (2011).
25. Wadati, H. *et al.* Revealing orbital and magnetic phase transitions in $Pr_{0.5}Ca_{0.5}MnO_3$ epitaxial thin films by resonant soft x-ray scattering. *New J. Phys.* **16,** 033006 (2014).
26. Van Veenendaal, M. Ultrafast photoinduced insulator-to-metal transitions in vanadium dioxide. *Phys. Rev. B* **87,** 235118 (2013).
27. Johnson, S. L. *et al.* Nanoscale depth-resolved coherent femtosecond motion in laser excited bismuth. *Phys. Rev. Lett.* **100,** 155501 (2008).
28. Harmand, M. *et al.* Achieving few-femtosecond time-sorting at hard X-ray free-electron lasers. *Nature Photon.* **7,** 215–218 (2013).
29. Herrmann, S. *et al.* CSPAD-140k: A versatile detector for LCLS experiments. *Nucl. Instrum. Methods A* **718,** 550–553 (2013).
30. Rodriguez, E. E., Proffen, Th., Llobet, A., Rhyne, J. J. & Mitchell, J. F. Neutron diffraction study of average and local structure in $La_{0.5}Ca_{0.5}MnO_3$. *Phys. Rev. B* **71,** 104430 (2005).
31. Amelitchev, V. A. *et al.* Structural and chemical analysis of colossal magnetoresistance manganites by Raman spectrometry. *Phys. Rev. B* **63,** 104430 (2001).

Acknowledgements

This work was supported by the NCCR Molecular Ultrafast Science and Technology (NCCR MUST), a research instrument of the Swiss National Science Foundation (SNSF). A.C. and T.K. acknowledge financial support by SNSF, Grants No. 200021_124496 and 200021_144115, respectively. Portions of this research were carried out at the Linac Coherent Light Source (LCLS) at SLAC National Accelerator Laboratory. LCLS is an Office of Science User Facility operated for the US Department of Energy Office of Science by Stanford University. Portions of this research received grants from the Japan Society for the Promotion of Science (JSPS) through the 'Funding Program for World-Leading Innovative R&D on Science and Technology (FIRST Program)', initiated by the Council for Science and Technology Policy (CSTP). This work was partially supported by the Ministry of Education, Culture, Sports, Science and Technology of Japan (X-ray Free Electron Laser Priority Strategy Program).

Author contributions

U.S., S.L.J. and P.B. conceived the experiment; A.C., S.O.M., S-W.H., C.D., H.W., H.T.L., M.C., G.I., T.H., J.A.J., A.F., T.K., M.R., S.L.J., U.S. and P.B. carried out the experiment; H.T.L., M.C., D.Z., J.M.G., M.S. and A.R. set up and operated the beamline including the optical pump laser; A.C., S.O.M., J.A.J., C.D., T.H. and H.T.L. analysed the data online during the experiments; A.C. analysed the data; H.W., M.N., M.K. and Y.T. conceived, designed and characterized the sample; S.O.M., L.R., A.C. and U.S. performed the static diffraction experiments; P.B. developed the model and performed the simulations with input from S.L.J.; P.B., S.L.J. and U.S. wrote the manuscript with discussions and improvements from all authors.

Additional information

Supplementary information is available in the online version of the paper. Reprints and permissions information is available online at www.nature.com/reprints. Correspondence and requests for materials should be addressed to P.B.

Competing financial interests

The authors declare no competing financial interests.